Supplementary Material:

Preparation of 4D Printed Peripheral Vascular Stent and its Degradation Behavior under Fluid Shear Stress after Deployment

*Xianli Wang [a,b], Yue Zhang [a,b], Peiqi Shen [a,b], Zhaojun Cheng [a,b], Chenglin Chu [a,b], Feng Xue, [a,b] and Jing Bai [a,b,]**

[a] *School of Materials Science and Engineering, Southeast University, Jiangning, Nanjing 211189, Jiangsu, China;*

[b] *Jiangsu Key Laboratory for Advanced Metallic Materials, Jiangning, Nanjing 211189, Jiangsu, China*

***Corresponding authors:**

Associate Prof. Jing Bai; Email: baijing@seu.edu.cn

➢ 1 The revolution of polymer commercial stent.

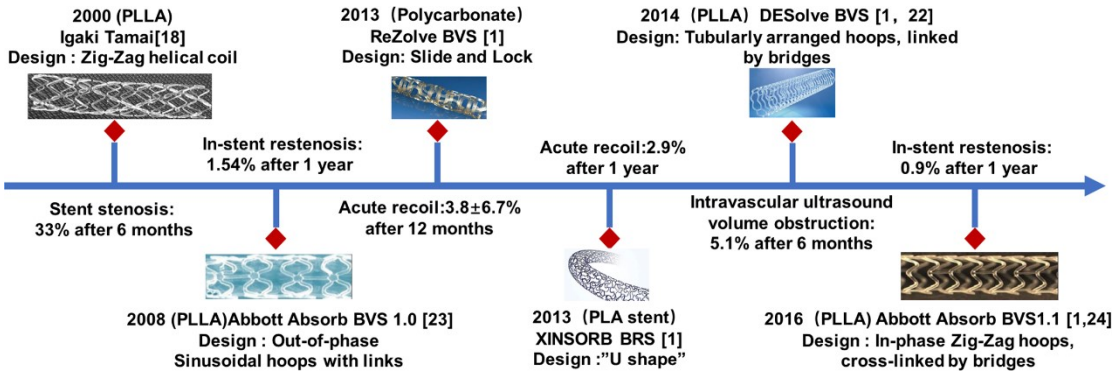

Fig.S1 Current commercial progress into bioresorbable polymer stents (Abbreviations: Poly (L-lactic acid) (PLLA), Bioresorbable Vascular Scaffold (BVS), Bioresorbable stent: (BRS)).

➢ 2 Evaluation of the extruded PLA filament

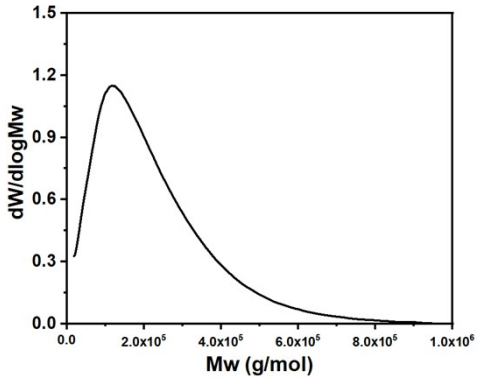

Fig.S2 GPC curves of macromolecules in PLA stent after preparation.

As determined by GPC, the weight average molecular weight (M_w), number average molecular weight (M_n), and PDI of the polymer after degradation were 13.8×10^4 g/mol, 7.8×10^4 g/mol, and 1.77, respectively.

➢ 3 The influence of printing parameters.

Dumbbell shape samples with 0.4mm-thick and a layer thickness of 0.1, 0.2, and

0.4mm, respectively, were printed under the guide of ASTM D 638-14 for the tensile test with a rate of 5 mm/min until failing, aimed to study the influence of interlayer defects on the mechanical strength of the 4D printed device.

Among all parameters in printing, layer thickness affects the strength of 4D printed devices significantly. The Elastic modulus of the three plates with a thickness of 0.4 mm is ~2187 MPa (layer thickness =0.1 mm), ~2290 MPa (layer thickness =0.2 mm), and ~2430 MPa (layer thickness =0.4 mm), respectively, as reflected in **Fig.S3(a)**. Decrement of Elastic modulus with layer thickness decreasing is mainly ascribed to the defects **Fig.S3(b)** and poor interlaminar adhesion caused by layer-by-layer stacking. As a result, the strength of a single-layer stent is better than that of a multi-layer one when the wall thickness is the same (0.4 mm wall thickness) (**Fig.S3(c)**). Therefore, in the following stent design, all stents were composed of a single layer (**Fig.S3(d)**).

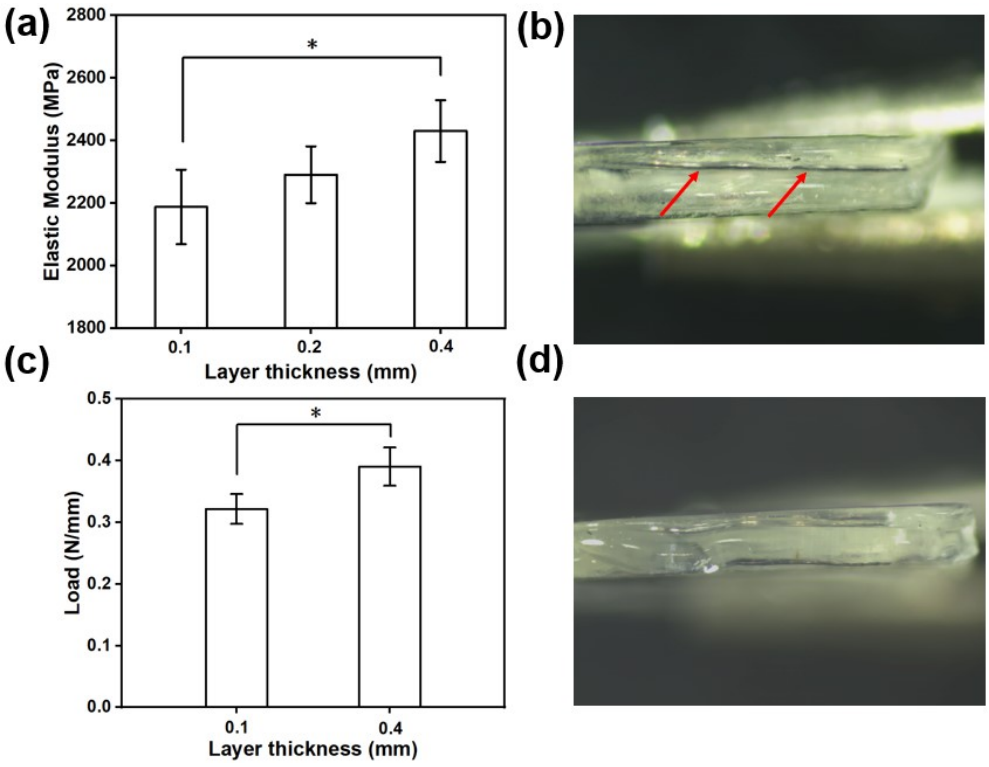

Fig.S3 (a) Elastic modulus of dumbbell shape plates with 0.4-mm thick but different

layer thicknesses. **(b)** Cross-section image of the multi-layer plate before wrapped under a stereoscopic microscope (red arrows point to the grooves between layers). **(c)** The compressive force of 0.4 mm-wall-thickness stents with a different layer thickness (n=4, *p<0.05). **(d)** Cross-section image of the single-layer plate before wrapped under a stereoscopic microscope.

➢ 4 Platelet adhesion

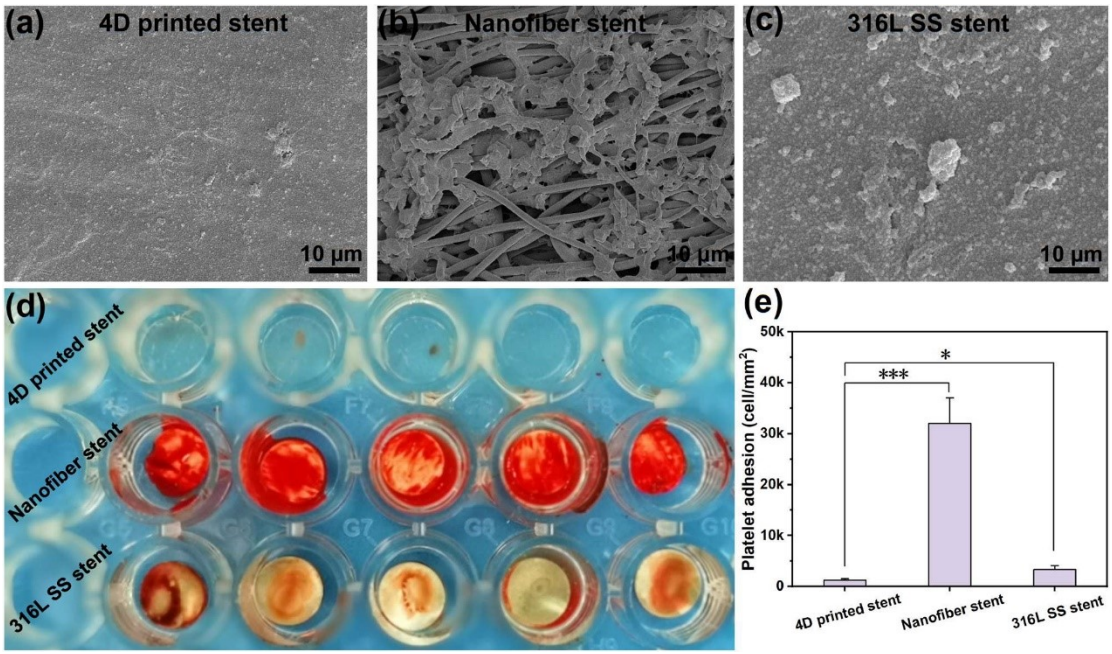

Fig.S4 (a) The optical images of thrombus generated on the sample surfaces. **(b)** Typical SEM images of platelets adhered on the sample surfaces after incubation in platelet-rich plasma in PRP for 2 hours. **(c)** The number of the platelets adhered on the 4D printed stent, 316L SS stent, and nanofiber stent (n=6, * $p < 0.05$, *** $p < 0.001$).

After incubated in platelet-rich plasma for 1 h, we found that only a small number of platelets adhered to the disk punched by the same material of the 4D printed stent (PLA), while the PLA nanofiber disks and the 316L SS disks as the control group had

significantly more platelets adhered to the PLA disks (*p<0.05).

➢ 5 Mechanical properties of the 4D printed stent with different wall thickness

➢ 5.1 The relationship between compression force and stent wall thickness

It is noted that the compressive forces are non-linear as a function of thickness. Under the plate compression load, the PLA thin-walled tube first undergoes a transient elastic stage (Stage II) and then enters the platform stress stage (Stage III) when the deformation is 50%. When large deformation occurs, the tube would form a plastic hinge on the upper, lower, left, and right walls under the effects of plate compression, and its deformation mechanism is shown in **Fig.S4**, which is generally a four-hinge structure. In the whole compression process, the compression load (F) of the tube can be expressed as follows [1]:

$$F = \begin{cases} \alpha S \delta & \delta \le \delta_D \ (Eq.S1) \\ \dfrac{2\alpha\sigma_y L t^2}{D\sqrt{1-\left(\dfrac{\delta}{D}\right)^2}} & \delta > \delta_D \ (Eq.S2) \end{cases}$$

Where α is the size coefficient of the thin-walled tube, S is the stiffness of the ring, δ_y is the yield strength of PLA bulk. L, t, D is the length, wall thickness, and average diameter of the thin-walled tube. δ is the compression displacement of the tube and δ_D is the compression displacement of the elastic end. According to **Eq.S2**, the plate compression load of the thin-walled tube is proportional to the square of its wall thickness (t), which is also applicable to our 4D printed stent.

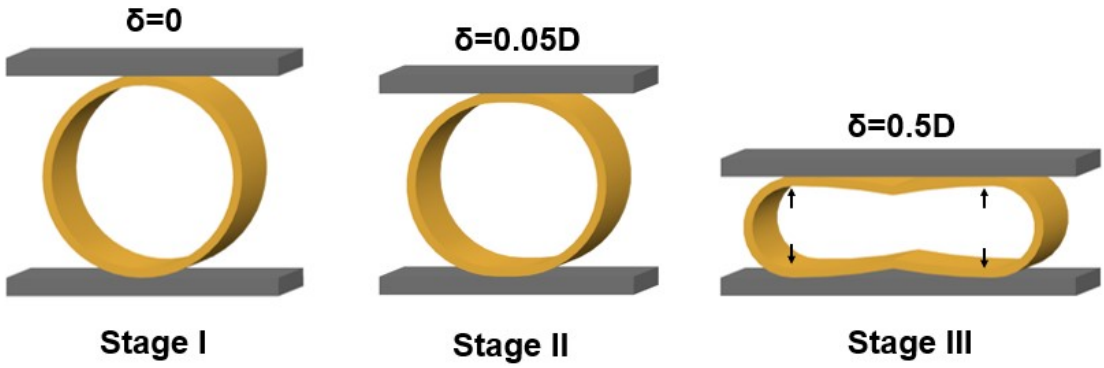

Fig.S5 The deformation process of thin wall tube under plate compression force.

➢ 5.2 Anti-fatigue resistance of stent with different wall thickness

The inserts in **Fig.S5(a)-(c)** present the cross-section images of stents after 100 cycles of compression fatigue tests. It can be found that stents with a wall thickness of 0.2 and 0.3 mm still keep their original shape, while the 0.4 mm one deforms significantly. Additionally, **Fig.S6(a)-(c)** show the cyclic Load-Strain curves. After calculation, the compression force decrements are ~6%, ~9%, and ~15%, and the recovery ratio losses are ~5%, ~14%, and ~21%, respectively, for 0.2 mm, 0.3 mm, and 0.4 mm stent, when compared to those before compression. The 0.2 mm and 0.3 mm wall-thickness stents show good elasticity and fatigue resistance after 100 cyclic deformations, which is attributed to the lower elastic modulus of PLA. Moreover, the happening time of force decaying and hysteresis phenomena is advanced with the wall thickness increasing, especially for the 0.4 mm one (**Fig.S6(c)**). That is because plastic deformation happened and the stent could not recover to its original shape anymore.

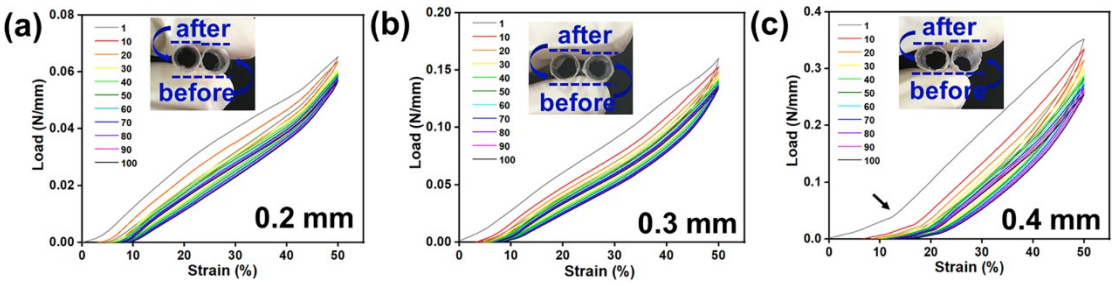

Fig.S6 Cyclic Force vs. Compression (%) curves of stents after shape memory recovery with different wall thicknesses before and after compressed (Inserts show the cross-section images).

➢ 6 The influence of deployment temperature on the stent mechanical properties

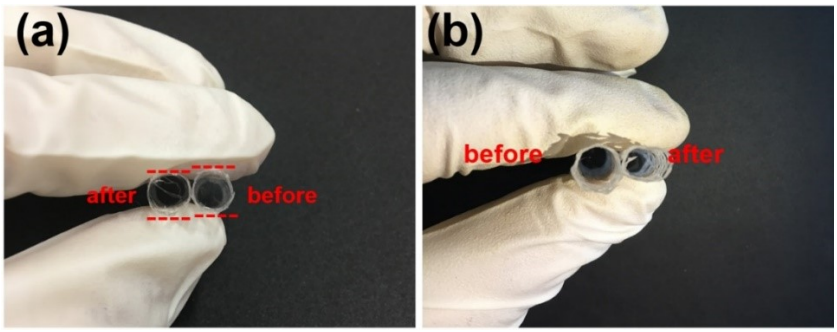

Fig.S7 Cross-section of the stent after **(a)** recovering from the water at 60 °C and **(b)** 50% a radial contraction at 37 °C.

Fig.S7(a) shows the stent can recover to almost its original diameter at 60 °C and **Fig.S7(b)** shows that after 50% radial contraction at 37 °C, the stent collapses.

➢ 7 In vitro degradation test design

(1) The stents were immersed in PBS without any other process, and the volume of PBS to the stent surface area was 50 ml/cm^2 in the guide of the standard.

(2) A homemade contracting machine was used to contract the stent to the 2-fold radial reduction in a water bath (60±0.5°C) at a moderate rate of 0.05 mm/s. Thereafter, the stent was fixed in icy water for 5 s, and then it was implanted in a soft silicone tube with an inner radius of 6.5 mm to prevent stent shifting, followed by transient

heating (60 °C) for 1min to activate the stent to its virgin shape. **Video S1** shows the shape memory effect of the 4D printed stent and the size change is less than 0.2 mm. Then the stents were immersed in PBS proportionally.

(3) Stents without any other post-processing were implanted into soft silicone tubes. Then the tubes were connected to a high-precision peristaltic pump (Huiyu fluid equipment co., Ltd., Beijing, China). The pump output fluid form is sinusoid and the maximum flow velocity is ~600 mL/min. Herein, the average liquid flow is within the range of healthy arterial blood flow [2].

(4) The post-process applied on the 4D printed stent is the same as Condition 2. Differently, after being implanted into a silicone tube, fluid was connected to the tube with the same velocity as Condition (3).

➢ 8 Finite Element Analysis

➢ 8.1 Model building

To calculate the shear stress applied by the fluid to the stent, the hemodynamic analysis was performed on the Fluid Solid Interaction systems by a combination of Static structural and Fluid Flow. The inner diameter, wall thickness, and length of the blood vessel model were 6.5 mm, 0.2 mm, and 60 mm, respectively. The inner surface of the blood vessel and the outer surface of the stent were defined as the Fluid-Solid interface and no slip happened. A linear elastic model with isotropy was adopted for the blood vessel, with a density of 1062 kg/m^3, an elastic modulus of 1.75 MPa, and Poisson's ratio of 0.495, respectively. The blood was treated as an incompressible

Newtonian fluid with a density of 1060 kg/m^3, dynamic viscosity of 0.0035 kg/m·s, and an inlet flow rate of 23 cm/s (equals to 386 mL/min), after that, flowed in the pattern of laminar flow [3-4]. Similarly, the blood vessel and stent were also meshed into tetrahedral grids, composed of 392,400 and 121,300 elements, respectively. The shear stress of the stent was got after 300-time iterations, all results were convergent and the residual of the momentum equation was 10^{-5}. Under the action of blood flow, the inner wall of the stent showed a distribution of wall shear stress (WSS).

➢ 8.2 Hydromechanics results

It has been reported that endothelial tissues began to cover the polymeric stent after post-operation for one month, and it may be completely covered after three months[5]. Therefore, it is meaningful to study the effect of fluid shear stress on stent degradation within two months after stent implantation. Once the stent is implanted, plasma particles strike the stent wall and they rebound at a clutter random angle because of the friction effect, which results in the distribution of WSS from all directions. Under the impact of blood flow with an average velocity of 382 mL/min, the absolute value of WSS on the inner wall of the stent is above 0.5 Pa (**Fig.S8**), which exceeds the critical value to induce In-stent Restenosis (ISR) [3]. From the view of hydromechanics, when the fluid flows in the pattern of laminar flow in a tube, the particles in the fluid move along the pipe axis, and the shear stress along the radial direction of the pipe is proportional to $1/R^3$ (where R is the distance of the particle to the axis) [6]. This means the velocity of flow and wall shear force near the wall of the tube is the smallest among the space of lumen. Once the fracture fragments fall off from the stent, they can be

washed away by the blood immediately, thus effectively reducing the possibility of ISR.

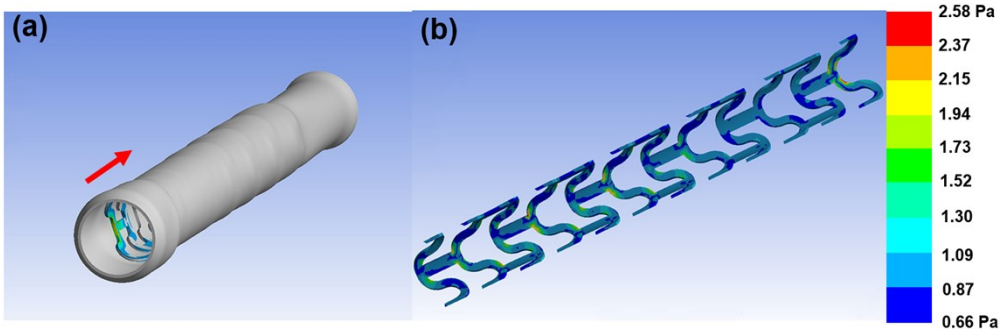

Fig.S8 Shear stress suffered by the stent calculated by Fluid Solid Interaction systems. **(a)** The direction of blood flow. **(b)** The absolute value of wall shear stress distribution on the inner surface of the stent.

➢ 9 In vitro degradation properties

Fig.S9 Representative "Y"-shaped units of stent wreckage after degraded for 8 weeks.

The image shows peak edges of the stent are the weak points of the stents and they are prone to break first because of stress concentration.

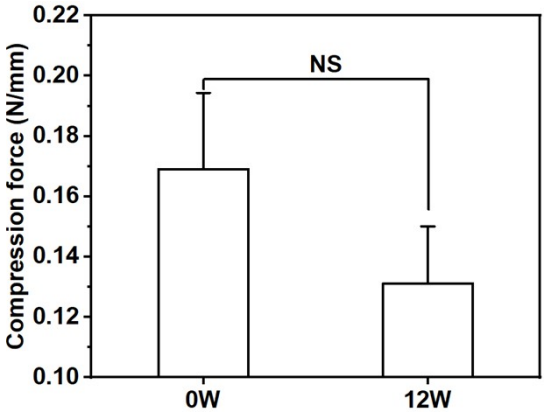

Fig.S10 Compression force of the 0.3 mm stent before and after degraded in NS for 12 weeks.

Fig.S10 shows that even after being immersed in a static environment for up to 12 weeks, the compression force of the stent did not reduce significantly. It indicates that the hydrolysis of PLA under a static system is much slower than the other degradation condition we discussed.

Video S1. The shape recovery process of our 4D printed stent.

➢ References

1. Tang Z, Li J, Zhu X, Journal of Materials Science & Engineering, 2016, **34**(04), 590-595.

2. Koo Y, Lee H, Dong Z, Kotoka R, Sankar J, Huang N, Yun Y, Sci. Rep.-UK, 2017, **7**(1)

3. Morlacchi S, Keller B, Arcangeli P, Balzan M, Migliavacca F, Dubini G, Gunn J, Arnold N, Narracott A, Evans D, Lawford P, Ann. Biomed. Eng., 2011, **39**(10), 2615-2626.

4. Barakat A I,Ann. Biomed. Eng., 2005, **33**(4), 444-456.

5. Guo Q, Lu Z, Wang J, Li T, J Mater Sci: Mater Med, 2011, **22**(6), 1615-1623.

6. Wang J, Jang Y, Wan G, Giridharan V, Song G, Xu Z, Koo Y, Qi P, Sankar J, Huang N, Yun Y, Corros. Sci., 2016, **104**, 277-289.